

On The Use of Eddy Current Brakes as Tunable, Fast Turn-On Viscous Dampers For Haptic Rendering

Andrew H. Gosline*

Gianni Campion†

Vincent Hayward‡

Haptics Laboratory, Center for Intelligent Machines, McGill University, Montréal, Canada

ABSTRACT

We describe the use of eddy current brakes as fast turn-on, tunable, linear dampers for haptic rendering using a prototype haptic device outfitted with eddy current brakes. We show that at the speeds typically required for haptic interaction, eddy-current-induced drag is proportional to velocity. We also show that a modulation rate of approximately 250 Hz can easily be achieved with off the shelf components. A method for decoupling the damping at the end effector is discussed. We discuss the results from haptic experiments for rendering viscosity, virtual walls and virtual friction. Experimental results show that the addition of programmable physical damping improves impedance and stability for rendering with negligible computational cost.

1 INTRODUCTION

Haptic interface technology is a growing field of research in science, engineering, and industry. With new demand for interfaces in areas such as medical training, manufacturing, human-computer interaction, and perception research, the desire for high fidelity haptic interfaces increases steadily. Naturally, the haptic interface hardware itself plays a large role in the fidelity of the interaction that a user can experience. Most haptic interfaces use active elements, such as electric motors, to drive a linkage. Typically, dissipation is an accidental by-product of their design. Uncontrolled and uncertain dissipation arises from various origins (dry friction, viscosity, electric, magnetic) in the motors and the drives used for torque amplification and/or transmission.

Recently, the benefits of tunable passive elements have been investigated by several authors. Cho *et al.* described a passive haptic display using only brakes to display virtual surfaces [5]. While completely passive displays have advantages, these come with the loss of key abilities such as programming responses in arbitrary directions. Clearly, a combination of active and passive actuators promises a wider range of rendering abilities which no device having actuators of only one kind could provide.

Kwon and Song describe a recent 2 DOF hybrid haptic interface using magnetorheological (MR) particle brakes [16]. An and Kwon discuss the use of MR brakes in a 1 DOF hybrid device as programmable dampers for haptic rendering [1]. MR particle brakes are programmable, but have a slow turn-on time [9], are nonlinear, and suffer from hysteresis as a result of demagnetization [14, 3]. Mehling *et al.* [20] shunt a DC motor with a capacitor and resistor in series to create frequency-dependent electrical damping. Their method, which essentially dissipates high frequency energy out of the motors to prevent limit cycles, is not programmable. In prior work, it is shown that physical damping can improve stability, but these methods for creating damping have important limitations.

We propose the use of an alternate passive actuation method based on eddy current brakes because they are inexpensive, friction-

free, capable of fast turn-on time, and linear. In this paper, we will briefly introduce the physics of eddy current braking, characterize the damping behavior of eddy current brakes, describe a method to compensate for the dynamic coupling that damped joints generate, and discuss results from haptic renderings of viscosity, virtual walls, and friction that use programmable physical damping.

2 EDDY CURRENT BRAKING

Eddy current brakes are simple magnetic devices that consist of a non-ferromagnetic conductor that moves through a magnetic field. An example is shown in Figure 1 where a magnetic field is created in the gap of a toroidal electromagnet, with diameter D . When the conductive disc rotates, eddy currents are induced at an average distance R from the axis of rotation where the pole's magnetic field moves as a function of the angular velocity of the disk.¹ Power is dissipated in the conductive disk by the Joule Effect, which creates a viscous-like torque applied to the disk.

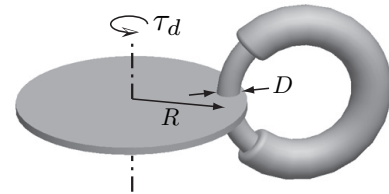


Figure 1: Tunable eddy current brake. A solid disc moves in the B field created by a toroidal electromagnet.

The physics that describe the power dissipation of an eddy current brake are non-trivial [10]. However, with certain assumptions, they can be simplified to investigate the underlying relationships. Neglecting the effect of the air gap, assuming a uniform cylindrical magnetic flux, and assuming that the magnet core is sufficiently smaller than the radius of the disc, the induced current density, J , in the conductive disc is a function of the angular velocity of the disk, $\dot{\theta}$, of the specific resistivity of the conductor, ρ , and the magnitude of the magnetic field, B [23, 18]:

$$|J| = \frac{1}{\rho} R \dot{\theta} |B|. \quad (1)$$

The power dissipated by the eddy current can be computed by integrating over the cylindrical volume such that:

$$P_d = \frac{\pi}{4\rho} D^2 dB^2 R^2 \dot{\theta}^2, \quad (2)$$

where d is the disc thickness and D is the diameter of the magnet core. Then, the braking torque is:

$$\tau_d = \frac{P_d}{\dot{\theta}} = \frac{\pi}{4\rho} D^2 dB^2 R^2 \dot{\theta}. \quad (3)$$

¹Also known as a "Foucault currents".

*e-mail: andrewg@cim.mcgill.ca

†e-mail: champ@cim.mcgill.ca

‡e-mail: hayward@cim.mcgill.ca

According to Eq. (3), the braking torque based on the aforementioned assumptions should vary linearly with the angular velocity and quadratically with the magnetic field. As the velocity becomes large, however, the eddy currents become large, and the magnetic field created by the induced eddy currents also become large and begin to counteract the magnetic field generated by the electromagnet. As a result, when the velocity is sufficiently high, the resulting drag no longer varies linearly with velocity [2]. Wiederick et al. suggest that there is a characteristic velocity, v_c , that denotes the velocity at which the magnetic field created by the eddy currents can no longer be neglected, thus making the damping nonlinear [24]:

$$v_c = \frac{2}{\sigma\mu_0 d}. \quad (4)$$

The quantities σ , μ_0 , and d are the conductivity, permeability, and thickness of the disc respectively. In later work, Marcuso et al. refer to this number when reporting results that illustrate the linear behavior of the eddy current damping at velocities well under the characteristic velocity [19]. For the aluminum disc used in their work, approximately 3.1 mm (1/8 inch) thick, v_c would correspond to approximately 19 ms^{-1} . In this work, the disc thickness is 1/16 inch, so v_c would be approximately 38 ms^{-1} , which results in a critical velocity which is safely above the normal operating conditions for a haptic device.

3 PROTOTYPE HAPTIC DISPLAY

A prototype haptic display that incorporates eddy current brakes has been constructed using the Pantograph haptic device as a test-bed [4]. Figure 2 shows the complete setup. An aluminum blade has been added to each proximal arm of the Pantograph such that blades rotate concentrically about the motor axis. This ensures that the brake acts at a constant radius throughout the workspace. Aluminum was chosen as the damper blade material because it has both good electrical conductivity to improve eddy current flow, and low specific density to keep inertia down. The damper blade inertia was minimized by cutting out all aluminum except for an annular section at the maximum radius. Identical toroidal electromagnets were constructed with a core machined out of iron and wrapped with 24 gauge enamel coated wire coils. A thin slot was cut through each core to allow the damper blades to pass through the magnet with a minimal air gap. Each magnet is driven in current mode by a Quanser LCAM that is powered by a 48 V power supply [12].

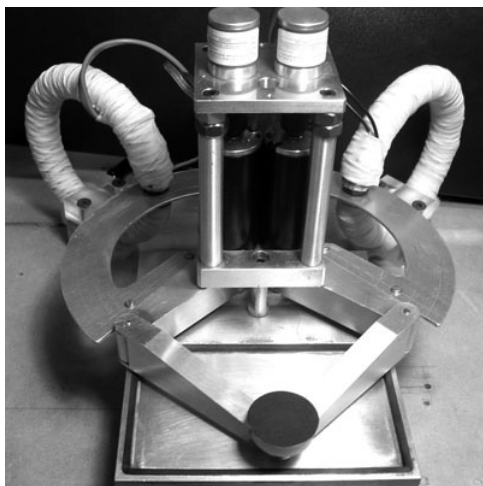


Figure 2: Prototype haptic 2 DOF display with two eddy current dampers.

4 EXPERIMENTAL VALIDATION

Apart from being friction free and inexpensive, there are two important characteristics of eddy current brakes that make them ideal viscous dampers for haptic interfaces. First, they can be turned on and off at high frequency, and second, their damping characteristics are linear with respect to velocity. This section investigates both characteristics.

4.1 Turn-on Time of Electromagnets

An important factor when designing a haptic interface is the system update rate. Because human touch is exquisitely sensitive to vibrations, it is important to update the force command such that the discrete nature of the signal becomes imperceptible. Although the required update frequency for a haptic interface to render smooth output is subject to many factors, it is generally accepted that the update rate should be *at least* several hundred Hz [7]. Since we intend to use the eddy current damper in a programmable fashion on a haptic interface, it is important that the damper be able to achieve a high update rate so damping can be modified within a sampling period.

Figure 4.1 shows the current response from 2 A step and then from a -2 A step commands into the current amplifiers. The results indicate a rise time of approximately 2.6 ms and a fall time of approximately 1.5 ms, making the maximum update rate of the damping system approximately 250 Hz. Due to the inductive nature of the impedance of an electromagnet, the amplifier was in saturation for the majority of the transient. Clearly, the turn-on time could be reduced by using an amplifier with a higher driving voltage or by modifying the magnetic circuit design. However, the discussion on the optimization of the magnetic design is outside the scope of this paper.

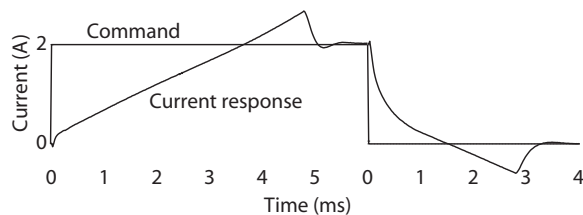


Figure 3: Current response to step commands.

4.2 Linear Properties of Eddy Current Damping

It is evident from the literature that eddy current brakes behave linearly at low speeds. However, in order to make the most of the damping characteristics, linearity must be investigated and the damping coefficient identified. We have performed experiments, using energy balance and torque balance approaches, to ascertain the properties of eddy current brakes at velocities that are typical of haptic interactions. The apparatus consisted of the proximal of the Pantograph with the damper blade attached to the arm such that it forms a concentric arc around the axis of the motor, as shown in Figure 4. This system was modeled as a mechanical system with a virtual torsional spring K (programmed with the torque), a moment of inertia J , friction in the bearings/motor τ_f , and viscosity $b(i)$ which is governed by:

$$J\ddot{\theta} + b(i)\dot{\theta} + K\theta = \tau_f(\theta). \quad (5)$$

In the energy balance approach, we considered the energy in the system for trajectories between rest positions to find all the desired

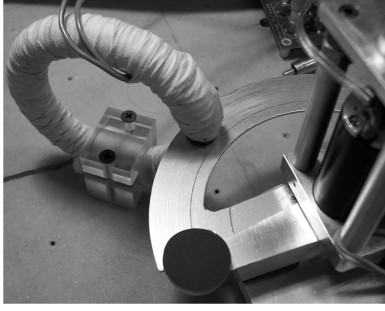


Figure 4: Apparatus for characterization of eddy current dampers.

unknowns from (5). We first estimated the energy lost by dry friction to find a correction term for the final energy balance. In the initial position, the damper was turned off, and a virtual spring, K_a , was deflected through a known angle, θ_a . The total energy of the system in the initial position was $E(K_a) = \frac{1}{2}K_a\theta_a^2$. In the final position, the virtual spring returned to its zero position, thus all the stored energy stored in the virtual spring was dissipated by friction:

$$E(K_a) = E_{\text{fric}}, \quad (6)$$

$$\frac{1}{2}K_a\theta_a^2 = \int \tau_{\text{fric}}(\theta)d\theta, \quad (7)$$

where E_{fric} was the energy dissipated by friction over the angle θ_a . In order to find the sought correction term, with the aid of the computer, a binary search method was employed, trying values of K_a until there was no overshoot. The procedure stopped when the test succeeded five times to resist outliers and the value of K_a was noted.

Now that the energy dissipated by friction over the angle θ_a was quantified, a second step was performed with the damper turned on. A new virtual spring constant K_d was found such that the damped system traveled from the same initial deflection, θ_a to the rest configuration with no overshoot either, using a similar method. The second energy balance gave:

$$E(K_d) = E_d + E_{\text{fric}}, \quad (8)$$

$$\frac{1}{2}K_d\theta_a^2 = \int \tau_d(\dot{\theta})\dot{\theta}(t)dt + E_{\text{fric}}, \quad (9)$$

$$\frac{1}{2}K_d\theta_a^2 = \int b\dot{\theta}(t)\dot{\theta}(t)dt + E_{\text{fric}}, \quad (10)$$

where $E(K_d)$ was the potential energy stored with the new spring constant, E_d the energy dissipated by the damper, and E_{fric} the energy lost to friction. Because E_{fric} was known from the first experiment:

$$b = \frac{\frac{1}{2}K_d\theta_a^2 - E_{\text{fric}}}{\int \dot{\theta}^2 dt}, \quad (11)$$

where $\int \dot{\theta}^2 dt$ was numerically integrated over the angle θ_a .

Results are shown in Figures 5 and 6 for deflections ranging from 0.06 to 0.8 Radians and coil currents of 0.4 to 4.0 Amps in 0.2 Amp increments. It is apparent from Figure 5 that the damping coefficient was almost constant irrespective of the angular deflection, which supports the theory that the eddy current brakes generate a dissipative torque that is linearly proportional to velocity at low speeds.

Figure 6 shows the damping coefficient of the brakes versus the coil current. According to the simplified theory, the eddy current torque should vary quadratically with current because the magnetic field is ideally linearly proportional to coil current. González attributes the lack of quadratic relationship in a similar experiment

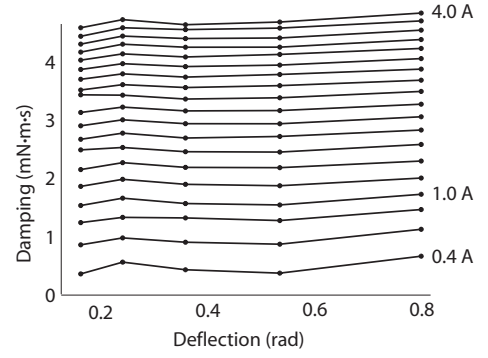


Figure 5: Damping Coefficient vs. Deflection.

to the non-linearities that occur with an iron core [10]. In addition, there are several other factors that can affect this relationship including heat, pole shape, air gap, and conductor boundary conditions [23]. In the case of an annular blade, the eddy currents have only a fixed volume of conductor in which to flow, which could certainly explain why the relationship appears to approach an asymptote, or a saturation point.

A second experiment was performed to verify the damping coefficient to coil current relationship using a terminal velocity torque balance. A similar saturation-like trend was found with the damping coefficient asymptotically reaching approximately 6 mN·m·s. The torque balance method has a limited range of use, given hardware constraints that allow for approximately 150 degrees of rotation. This leads to a small range of suitable terminal velocities, which is why the torque balance method was used only to verify the energy balance results.

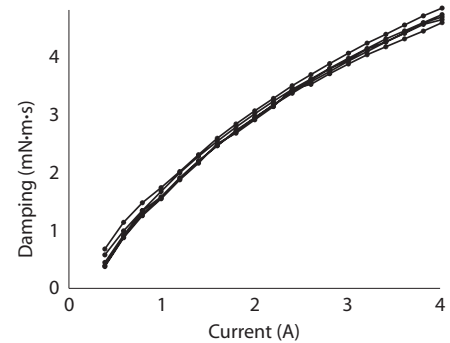


Figure 6: Damping Coefficient vs. Coil Current for different deflections amplitudes.

The experiments conducted with the virtual spring and terminal velocity tested the linearity of the damper on a range of velocities that covers the usual exploration speed of a human user [17]. The maximum angular velocity achievable by the device with its torques is approximately 35 rad/s when no damping is used. According to [17], usual interactions with haptic devices occur at speeds that are of order 500 mm/s at the manipulandum (approximately 20 rad/s at the Pantograph joints). We can safely assume that the eddy current brakes are within their linear range, because the magnetic characteristic velocity of the blades corresponds to approximately 600 rad/s, which exceeds the typical manipulandum speeds by more than an order of magnitude.

5 VISCOSITY RENDERING

To apply programmable physical damping techniques to haptic rendering, it is important to investigate how damping the joints affects the dynamics at the manipulandum. Because the damping torques are transferred to the manipulandum through the non-diagonal Jacobian matrix, J , of the device's kinematic map, the viscosity at the manipulandum will be neither homogeneous throughout the workspace, nor isotropic.

The force produced by the manipulandum is:

$$F_{xy} = J^{-T} \tau, \quad (12)$$

where τ is the vector of joint torques. The torques that result from the eddy current dampers are:

$$\tau = B_{\text{joint}} \omega, \quad (13)$$

where B_{joint} and ω are the diagonal damping matrix and joint velocity vectors respectively. Substituting Eq. (13) into Eq. (12), and substituting $\omega = J^{-1}v_{xy}$, the effect of damping the joints seen from the manipulandum can be expressed by [22]:

$$F_{xy} = J^{-T} B_{\text{joint}} J^{-1} v_{xy}. \quad (14)$$

It is evident from Eq. (14) that F_{xy} will suffer from coupling between directions and that the viscous forces in the workspace will in general not be aligned with velocity. In order to render arbitrary damping at the manipulandum, the motors can be used to compensate by nulling these parasitic forces [8]. Let B_{xy} be the damping matrix created at the manipulandum which is such that $F_{xy} = B_{xy}v_{xy}$:

$$B_{xy} = \begin{pmatrix} b_{xx} & b_{xy} \\ b_{yx} & b_{yy} \end{pmatrix}. \quad (15)$$

Solving Eq. (14) gives a value for a desired joint damping behavior B_{des} which in general is unachievable:

$$B_{\text{des}} = J^T B_{xy} J. \quad (16)$$

Let the Jacobian matrix entries be: $J = \begin{pmatrix} a & b \\ c & d \end{pmatrix}$. We desire B_{xy} to be diagonal, with $b_{xy} = b_{yx} = 0$. Evaluating Eq. (16) gives

$$\begin{aligned} B_{\text{des}} &= \begin{pmatrix} a^2 b_{xx} + c^2 b_{yy} & ab b_{xx} + cd b_{yy} \\ ab b_{xx} + cd b_{yy} & b^2 b_{xx} + d^2 b_{yy} \end{pmatrix} \\ &= B_{\text{diag}} + B_{\text{off}}, \end{aligned} \quad (17)$$

$$(18)$$

where B_{diag} and B_{off} , are the diagonal and off-diagonal terms of the resulting B_{des} matrix. Substituting Eq. (18) into Eq. (13) give this command law [8]:

$$\tau_{\text{visc}}(t) = B_{\text{diag}}(t) \omega(t) + B_{\text{off}}(t) \bar{\omega}(t), \quad (19)$$

where the first term is implemented by commanding the physical joint viscous dampers, and the second term computed from the estimated angular velocities $\bar{\omega}$ and implemented by the motors.

It is clear that the rendering of viscous damping in the x, y workspace is not achievable by the dampers alone. The balance between the contributions of the diagonal and off-diagonal elements (of passive vs active origin) vary across the workspace and depend on the direction of the desired damping. For instance, the rendering of homogeneous damping is not guaranteed to be completely passive because the motors are required to provide a corrective torque. Preliminary experiments with control law (19) confirm nevertheless the beneficial effects of physical damping, even with active compensation.

The experiments in the next section were performed without compensation, because precise viscosity specification was not necessary to the rendering since, during free space exploration, damping was not needed. The dampers were used for the sole purpose of quenching limit cycles. However, for rendering pure viscosity, law (19) improves the feel noticeably.

6 PHYSICALLY DAMPED VIRTUAL WALL

Colgate and Schenkel related stiffness, damping, and update frequency required for the passive simulation of a virtual wall to the amount of physical damping that exists in the device [6]. From the expression they have developed, it is clear that achievable virtual stiffness is a function of the amount of physical damping present in the system. We have performed experiments with virtual walls and shown that the introduction of tunable damping indeed does stabilize a wall that would otherwise be active. The virtual wall had a virtual stiffness k_0 and was aligned along the y direction and located at $x = 0$. Elasticity was virtual and damping $\mathcal{B}(\omega)$ physical (3 mN·m·s applied to each joint). The dampers were turned on only when the manipulandum was inside the wall:

$$f_x(t) = \begin{cases} k_0 \bar{x}(t) + \mathcal{B}(\omega) & \text{if } x(t) > 0, \\ 0 & \text{otherwise,} \end{cases} \quad f_y(t) = 0. \quad (20)$$

Figure 7 shows the results from experiments with wall stiffnesses of 400 N·m⁻¹ and 1200 N·m⁻¹. These experiments were performed using a pre-tensioned elastic band to thrust the manipulandum into the virtual wall, and to hold it up against it in a reproducible manner.

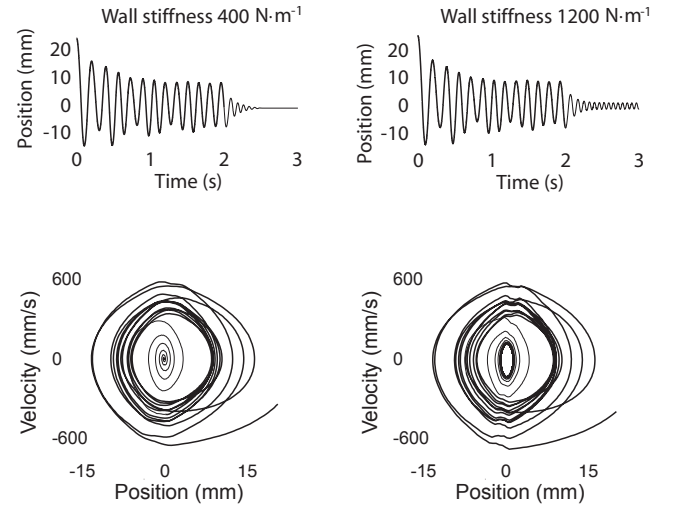


Figure 7: Results from Experiment with Physically Damped Virtual Wall.

To demonstrate the effect of the dampers, they were not used ($\mathcal{B}(\omega) = 0$) until $t = 2$ s (shown by a thinner plot line). It is clear that once the system received physical damping, the limit cycle present in the 400 N·m⁻¹ case was quenched, while the limit cycle in the 1200 N·m⁻¹ was reduced in magnitude. It is important to note that the amplitude of the initial oscillations, when there is no damping, is very similar between the two walls, regardless of the programmed stiffness. This is due to amplifier saturation, which limits the maximum force that the device can exert. However, the walls behave linearly in the non-saturated regions close to the contact plane, and this is where the effect of the damping is the most evident. Also,

the reduced limit cycle in the $1200 \text{ N} \cdot \text{m}^{-1}$ case is within the linear region of the wall, and is therefore not affected by amplifier saturation.

7 PHYSICALLY DAMPED VIRTUAL FRICTION

Haptic rendering of friction is important for realism in virtual environments, and several computational friction models have been developed to make its simulation possible. One characteristic of computational friction models that can lead to unpredictable results is the model's dependence on velocity, such as the popular Karnopp model [15], or the more recent damped-spring method proposed by Nahvi *et al.* [21]. Accurate velocity estimation is problematic because it is in conflict with high update rates [13].

Hayward and Armstrong developed a computational a stick-slip model of friction that is "time free", and hence does not require the computation of velocity to render friction [11]. This model, however, in its most basic form, does not specify any dissipation in the stuck regime and hence is prone to limit cycles when there is not sufficient physical damping in the device. With the addition of programmable physical damping, it is possible to add damping in the stuck state, and optionally, turn it off when in the sliding state, thus improving stability without any dependence on velocity estimation.

The model computes a friction force based on the position $x(t)$ of a simulated sliding object and on the position $w(t)$ of an anchor. The deflection $z(t) = x(t) - w(t)$ is used to determine a friction force. The model is such that at all times these equations hold:

$$f(t) = \begin{cases} \sigma_0 [z(t)/z_{\max}] & \text{stuck if } |z(t)| < z_{\max}, \\ \sigma_0 & \text{otherwise sliding,} \end{cases} \quad (21)$$

where z_{\max} is a user defined characteristic length that determines the transition from sticking to slipping. The vectorial version of this model was used in the experiment [11].

When the object is in the stuck state, friction force is purely elastic. Damping may be added according to:

$$b(t) = \begin{cases} \mathcal{B}(\omega) [1 - (|z(t)|/z_{\max})] & \text{stuck if } |z(t)| < z_{\max}, \\ 0 & \text{sliding otherwise.} \end{cases} \quad (22)$$

An experiment was carried out by asking a user to touch the manipulandum, sliding it left or right, and releasing it in a regular pattern. The sequence of events was: (a) touch, (b) slide, (c) release, touch, slide, release, and so-on. It is evident from Figure 8a that a limit cycle kicks-in when the user's finger is removed, but vanishes during sliding.

In Figure 8b, physical damping was added in the joints according to the law (22). The limit cycle that occurred when the finger was removed from the manipulandum was quenched by damping shortly after the release of contact. This experiment shows how little physical dissipation was present in the Pantograph. Being entirely made of aluminum, all pivots using precision ball bearings, and using torquers in a direct drive configuration, very little vibration energy was dissipated in the Pantograph alone. For this experiment, $\sigma_0 = 0.5 \text{ N}$ and $z_{\max} = 1 \text{ mm}$.

8 CONCLUSION

A prototype haptic interface with tunable eddy current dampers has been designed and built. A brief discussion of eddy current brake theory was presented to familiarize the reader with their physical behavior and underlying relationships. Experiments were performed to characterize the nature of the damping generated by eddy current brakes. In accordance with the theory, the damping from eddy current brakes was found to be linearly dependent on velocity.

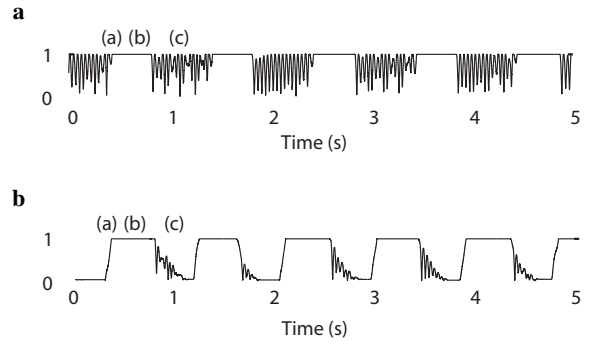


Figure 8: Normalized deflection. a) without physical damping. b) with damping according to law (22).

A method was developed and tested that compensates for kinematic coupling in order to null parasitic manipulandum forces that result from damping from the motorized joints of the device. This method could be easily extended to any haptic device provided that they are reasonably kinematically conditioned.

The benefits of programmable eddy current damping in haptic rendering have been then investigated with virtual wall and virtual friction experiments. The addition of eddy current damping allowed for a stable rendering of virtual viscosity, a virtual wall and virtual friction when the wall and friction models were shown to be unstable without it.

Despite the encouraging results, much future work remains to be done. Firstly, the damper blades add significant inertia to the device, and future design iterations will attempt to optimize the trade-off between inertia and damping torque. Secondly, because the rise time of an electromagnet is simply a function of its inductance, it should be relatively easy to achieve a faster turn-on time with amplifiers that can deliver a higher driving voltage than the ones used in this work. Moreover, there exist many other magnetic device design geometries that could be more efficient, and improvement of the eddy current brake geometry and hardware is ongoing work.

We believe that eddy current brakes, for example with a configuration similar to that of Figure 1, could easily be retrofitted on existing haptic devices that employ joint torquers, such as electric motors. Also, in devices which employ torque amplification, the damping torque would also be amplified by the transmission, yielding an effective damping that would increase quadratically with the transmission ratio.

Finally, in this work, programmable damping has been added to haptic renderings only to stabilize the system and improve the impedance range of the device. A major goal for future work is to use programmable analog damping in rendering of textures, deformable objects, contact, and to use the dampers as dissipative elements in future passivity-observer control schemes.

9 ACKNOWLEDGMENTS

This work was funded by a Collaborative Research and Development Grant "High Fidelity Surgical Simulation" from NSERC, the Natural Sciences and Engineering Council of Canada and by Immersion Corp., and by a Discovery Grant also from NSERC.

REFERENCES

- [1] J. An and D.S. Kwon. In haptics, the influence of the controllable physical damping on stability and performance. In *Proc. IROS 2005, IEEE/RSJ Int. Conf. Intelligent Robots and Systems*, pages 1204–1209, 2004.

- [2] S. Anwar. A parametric model of an eddy current electric machine for automotive braking applications. *IEEE Transactions on Control Systems Technology*, 12(3):422–427, 2002.
- [3] M. Arcy. Design of a single degree of freedom ‘mechanical bread-board’ haptic display. Master’s thesis, Northwestern University, 1996.
- [4] G. Champion, Q. Wang, and V. Hayward. The Pantograph Mk-II: A haptic instrument. In *Proc. IROS 2005, IEEE/RSJ Int. Conf. Intelligent Robots and Systems*, pages 723–728, 2005.
- [5] C. Cho, M. Kim, and J. Song. Direct control of a passive haptic based on passive force manipulability ellipsoid analysis. *International Journal of Control, Automation, and Systems*, 2(2):238–246, 2004.
- [6] J. E. Colgate and G. Schenkel. Passivity of a class of sampled-data systems: Application to haptic interfaces. In *Proc. of American Conference on Control*, pages 3236–3240, 1994.
- [7] S. Cotin and H. Delingette. Real-time surgery simulation with haptic feedback using finite elements. In *Proc. IEEE International Conference on Robotics and Automation*, 1998.
- [8] M. Doyon, V. Hayward, and M. Pelletier. Decentralized impedance control. In *Proc. International IFAC Symposium on Robot Control SYROCO’94*, 1994.
- [9] M. Gogola and M. Goldfarb. Design of a PZT-actuated proportional drum brake. *IEEE Transactions on Mechatronics*, 4(4):409–416, 1999.
- [10] M. I. Gonzalez. Experiments with eddy currents: The eddy current brake. *European Journal of Physics*, 25:463–468, 2004.
- [11] V. Hayward and B. Armstrong. A new computational model of friction applied to haptic rendering. In *Experimental Robotics VI, Lecture Notes in Control and Information Sciences*, pages 403–412. Springer-Verlag, 2000.
- [12] Quanser Inc. <http://www.quanser.com/>. World Wide Web Page.
- [13] F. Janabi-Sharifi, V. Hayward, and C-S. J. Chen. Discrete-time adaptive windowing for velocity estimation. *IEEE Transactions on Control Systems Technology*, 8(6):1003–1009, 2000.
- [14] C. L. Kapuscinski. Motor selection and damper design for a six degree of freedom haptic display. Master’s thesis, Northwestern University, 1997.
- [15] D. Karnopp. Computer simulation of stick-slip friction in mechanical dynamic systems. *Transactions of the ASME*, 107:100–103, 1985.
- [16] T.B. Kwon and J.B. Song. Force display using a hybrid haptic device composed of motors and brakes. *Mechatronics*, 16:249–257, 2006.
- [17] S.J. Lederman, R.L. Klatzky, C.L. Hamilton, and G.I. Ramsay. Perceiving roughness via a rigid probe: Psychophysical effects of exploration speed and mode of touch. *Haptics-E: Electronic Journal of Haptics Research*, 1, 1999.
- [18] K. Lee and K. Park. Optimal robust control of a contactless brake system using an eddy current. *Mechatronics*, 9:615–631, 1999.
- [19] M. Marcuso, R. Gass, D. Jones, and C. Rowlett. Magnetic drag in the quasi-static limit: Experimental data and analysis. *American Journal of Physics*, 59(12):1123–1129, 1991.
- [20] J. S. Mehling, J. E. Colgate, and M. A. Peshkin. Increasing the impedance range of a haptic display by adding electrical damping. In *Proc. of the First Joint Eurohaptics Conference and Symposium on Haptic Interfaces for Virtual Environment and Teleoperator Systems WHC’05*, 2005.
- [21] A. Nahvi and J. M. Hollerbach. Display of friction in virtual environments based on human fingerpad characteristics. In *Proc. of the Haptic Interfaces for Virtual Environment and Teleoperator Systems Symposium, ASME Dynamic Systems and Control Division*, volume DSC-Vol. 64, pages 179–184, 1998.
- [22] J. K. Salisbury. Active stiffness control of a manipulator in Cartesian coordinates. In *Proc. IEEE Decision and Control Conference*, pages 95–100, 1980.
- [23] E. Simeu and D. Geroges. Modeling and control of an eddy current brake. *Control Engineering Practise*, 4(1):19–26, 1996.
- [24] H. D. Wiederick, H. Gauthier, D. A. Campbell, and P. Rochon. Magnetic braking: Simple theory and experiment. *American Journal of Physics*, 55(6):500–503, 1987.